Using an MHD simulation to interpret the global context of a coronal mass ejection observed by two spacecraft

Pete Riley,[1] J. A. Linker,[1] Z. Mikić,[1] D. Odstrcil,[2] T. H. Zurbuchen,[3] D. Lario,[4] and R. P. Lepping[5]

Received 1 November 2002; revised 6 March 2003; accepted 18 April 2003; published 8 July 2003.

[1] In late February 1999 the ACE spacecraft observed a coronal mass ejection (CME) at 1 AU, in the ecliptic plane. Thirteen days later, Ulysses observed a CME at 5 AU and 22°S. We present a detailed analysis of the plasma, magnetic field, and composition signatures of these two events. On the basis of this comparison alone, it is not clear that the two spacecraft observed the same solar event. However, using a generic MHD simulation of a fast CME initiated at the Sun by magnetic flux cancellation and propagated out into the solar wind, together with additional evidence, we argue that indeed the same CME was observed by both spacecraft. Although force-free models appear to fit the observed events well, our simulation results suggest that the ejecta underwent significant distortion during its passage through the solar wind, indicating that care should be taken when interpreting the results of force-free models. Comparison of composition measurements at the two spacecraft suggests that significant spatial inhomogeneities can exist within a single CME. *INDEX TERMS:* 7513 Solar Physics, Astrophysics, and Astronomy: Coronal mass ejections; 7843 Space Plasma Physics: Numerical simulation studies; 2111 Interplanetary Physics: Ejecta, driver gases, and magnetic clouds; 2164 Interplanetary Physics: Solar wind plasma; 2169 Interplanetary Physics: Sources of the solar wind; *KEYWORDS:* coronal mass ejections, CMEs, MHD simulations, in situ observations

Citation: Riley, P., J. A. Linker, Z. Mikić, D. Odstrcil, T. H. Zurbuchen, D. Lario, and R. P. Lepping, Using an MHD simulation to interpret the global context of a coronal mass ejection observed by two spacecraft, *J. Geophys. Res.*, *108*(A7), 1272, doi:10.1029/2002JA009760, 2003.

1. Introduction

[2] Coronal mass ejecta (CMEs) are spectacular events involving the expulsion of significant amounts of solar material (10^{15-16} grams) into the heliosphere [*Hundhausen*, 1988]. Associated with this eruption is 10^{31-32} ergs of energy, which is presumably supplied by the magnetic field. However, the basic preeruption configuration and the topological changes in the magnetic field that result in the conversion of magnetic energy into kinetic energy are not well known. Undoubtedly, reconnection plays a central role, but the details of where it takes place, how fast, and for how long, are not well understood.

[3] A number of theoretical models have been proposed to explain the eruption and evolution of CMEs near the Sun. Useful reviews based on classification schemes are given by *Forbes* [2000] and *Klimchuk* [2001]. To varying degrees, all of these models are idealized and as such tend to focus on reproducing a particular aspect of the eruption process at the expense of others. In some cases this leads to model predictions that contradict reliable observations.

[4] Given the inherent complexity of CMEs, it is hardly surprising that theoretical models of CME eruption tend to be idealized. Nevertheless, if we are to make progress in understanding such phenomena, it is important to make connections between the models and observations. This may serve to place constraints on the models and may even differentiate between competing models, providing support for a particular physical mechanism.

[5] In this paper we analyze some of the interplanetary characteristics of a generic, 2.5-D (axisymmetric) simulation of the eruption of a flux-rope CME and its propagation and evolution through the inner heliosphere. Our goal is to connect the simulation results with in situ plasma, magnetic field, and composition measurements. We focus on a specific event that we believe was observed both at ACE and Ulysses in early 1999, which were located at significantly different radial distances and latitudes. We use the model results (as well as ancilliary information) to (1) argue that this was the same event observed at both spacecraft and (2) interpret the global context of the in situ observations. In the following section we introduce the MHD model. We

[1]Science Applications International Corporation, San Diego, California, USA.
[2]Space Environment Center, National Oceanic and Atmospheric Administration, Boulder, Colorado, USA.
[3]Department of Atmospheric, Oceanic, and Space Sciences, University of Michigan, Ann Arbor, Michigan, USA.
[4]Applied Physics Laboratory, Johns Hopkins University, Laurel, Maryland, USA.
[5]Laboratory for Extraterrestrial Physics, NASA Goddard Space Flight Center, Greenbelt, Maryland, USA.

0148-0227/03/2002JA009760

then discuss the in situ plasma, magnetic field, and composition observations of the February/March 1999 event in detail. We apply the so-called "force-free" fitting model to describe the basic features of the flux ropes at the two spacecraft and compare the in situ observations with the MHD simulation results. Finally, we discuss the implications of this analysis.

2. Description of the Model

[6] In this section we briefly describe the basic features of the coronal and heliospheric models and discuss their integration. A more detailed description has been provided by *Odstrcil et al.* [2002]. We solve the basic set of time-dependent, magnetohydrodynamic (MHD) equations that describe many aspects of the large-scale behavior of the solar corona and inner heliosphere. We separate the region of space into two parts, distinguishing between the "coronal" region, which spans the photosphere up to 20 R_S, and the "heliospheric" region, which spans 20 R_S to 5 AU. The SAIC coronal MHD model [*Mikić and Linker*, 1994] is used to solve for the coronal region and the NOAA/SEC heliosperic MHD model [*Odstrcil and Pizzo*, 1999a] is used to solve for the heliospheric region, being driven directly by output from the coronal solution. This approach has a number of practical and scientific advantages. In particular, each code has been designed specifically for its respective environment. Moreover, decoupling these regions in this way allows the heliospheric portion to run at significantly larger time steps than are required by the coronal algorithm.

[7] An important distinction between the present work and previous efforts to simulate CME propagation and evolution in the inner heliosphere concerns the location of the inner radial boundary. Previously, researchers typically placed this boundary at $20-30R_S$ to avoid numerical complications arising from the transition from subsonic to supersonic flow [e.g., *Riley et al.*, 1997; *Riley and Gosling*, 1998; *Odstrcil and Pizzo*, 1999a, 1999b; *Cargill et al.*, 2000; *Vandas et al.*, 2002]. This required, however, the specification of ad hoc perturbations to mimic the characteristics of the CME at this location. In fact, these perturbations were constructed in such a way so as to reproduce the observed solar wind observations at 1–5 AU. In contrast, our inner boundary is located at $1R_S$ and the flux-rope CME is initiated in a self-consistent fashion using a plausible (although not necessarily correct) mechanism. The subsequent evolution, through expansion and interaction with the ambient solar wind also proceeds self-consistently.

[8] The details of the algorithm used to advance the equations of the SAIC coronal model are given elsewhere [*Mikić and Linker*, 1994; *Lionello et al.*, 1998; *Mikić et al.*, 1999]. Here we make a few brief remarks. The equations are solved on a spherical (r, θ, ϕ) grid, which permits nonuniform spacing of mesh points in both r and θ, thus providing better resolution of narrow structures, such as current sheets. In the radial (r) and meridional (θ) directions we use a finite-difference approach. In azimuth (ϕ) the derivatives are calculated pseudospectrally. We impose staggered meshes in r and θ, which has the effect of preserving $\nabla \cdot \mathbf{B} = \mathbf{0}$ to within round-off errors for the duration of the simulation.

[9] The NOAA/SEC heliospheric model solves the time-dependent MHD equations in a spherical geometry using either the Flux-Corrected-Transport or Total-Variation-Diminishing schemes [e.g., *Odstrcil*, 1994; *Toth and Odstrcil*, 1996]. These high-resolution schemes produce second-order accuracy away from discontinuities, while simultaneously providing the stability that ensures nonoscillatory solutions. The numerical MHD code has been applied to a number of problems, such as detailing the interaction of fast and slow solar wind streams [*Odstrcil*, 1994], distortion of the HCS by shock waves [*Odstrcil et al.*, 1996], shock-induced magnetic reconnection of coronal sheets [*Odstrcil and Karlicky*, 1997], propagation of CMEs in a structured solar wind, [*Odstrcil and Pizzo*, 1999a, 1999b], distortion of the IMF by propagation of CMEs [*Odstrcil and Pizzo*, 1999c], propagation of shock waves in coronal structures [*Odstrcil and Karlicky*, 2000], and global dynamics of magnetic clouds [*Vandas and Odstrcil*, 2000].

[10] The SAIC coronal model, as implemented here, uses a polytropic index of $\gamma = 1.05$ to mimic the near-isothermal nature of the solar corona and thus produce plasma parameters that agree with observed values. On the other hand the NOAA/SEC code uses $\gamma = 5/3$ in agreement with the observed near-adiabatic nature of the solar wind. Ideally, one would like to implement a coronal model incorporating conduction, coronal heating, radiation loss, and Alfvén wave acceleration, together with $\gamma = 5/3$, to provide a seamless boundary between the two models. Unfortunately, practically speaking, such an approach is only now becoming feasible in two dimensions [*Lionello et al.*, 1999]. We have examined the boundary between the two models to estimate what artifacts may have been introduced by allowing γ to vary discontinuously across the boundary. Remarkably, with the exception of temperature (and hence thermal pressure), the magnetofluid parameters remain continuous. The plasma temperature profile with radial distance obviously changes abruptly at the boundary since $T \propto r^{-2(\gamma-1)}$. Thus in the coronal model, $T \propto r^{-1/10}$, whereas in the heliospheric model, $T \propto r^{-4/3}$. We are currently exploring improvements to the solar model to remove this artifcat. Nevertheless, our analysis suggests that the results will change only quantitatively.

[11] Solar rotation is incorporated into the model at the boundary between the coronal and the heliospheric models. It was neglected from the coronal model for simplicity, and we justify this approximation with the following argument. The Parker spiral angle at equatorial latitudes is given by $\phi_{Parker} = \tan^{-1}\left((2\pi/\tau)\int dr/v_r(r)\right)$, where τ is the solar rotation period (25.38 days), r is distance from the Sun, and v_r is the radial speed of the plasma, which near the Sun is a function of r. Assuming v_r = constant for simplicity, this reduces to the following convenient form: $\phi_{Parker} = \tan^{-1}(2r/v_r)$, where r is units of solar radii (R_S) and v_r is in units of kms^{-1}. For $r = 215$ R_S (=1 AU) and $v_r = 450$ kms^{-1} we find that $\phi = 44°$, as expected. For $r = 20R_S$ the field deviates from the radial direction by $\sim 5°$ and to a first approximation can be neglected. Thus to mimic the effects of solar rotation, we add an azimuthal component to the magnetic field of the coronal solution at the interface between the two codes as follows: $B'_\phi = B_\phi - 2B_r sin(\theta) r/v_r$.

2.1. Eruption of a Flux Rope CME

[12] The configuration of the solar corona prior to the emergence of the flux rope is summarized in the two

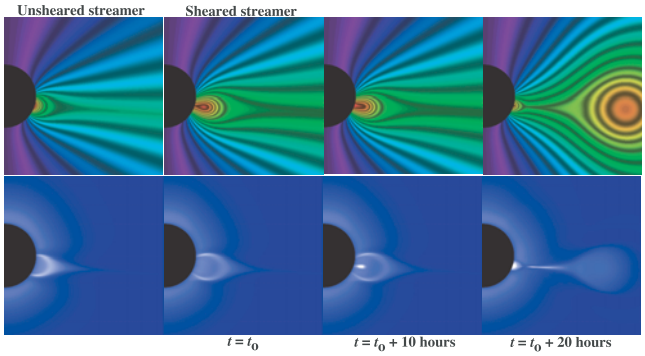

Figure 1. Evolution of a sheared helmet streamer via flux cancellation. Top panels show contours of the magnetic flux function, which in two dimensions are equivalent to the magnetic field. Bottom panels show simulated polarized brightness. The four columns summarize: (1) the state of the unsheared corona; (2) the sheared corona; (3) the eruption of the flux rope after 10 hours; and (4) the eruption of the flux rope after 20 hours, respectively.

leftmost panels of Figure 1. This type of equilibrium solution has been discussed in more detail by *Linker et al.* [1999]. Contours of the magnetic flux function (fiduciaries of magnetic field lines in two dimensions) are shown by the solid lines and shaded contours (top). The system consists of a single streamer belt displaced by $\sim 10°$ below the heliographic equator. The first column shows the state of the corona after the system has reached equilibrium. The second column shows how this configuration is modified by energization of the magnetic field via photospheric shear [*Linker and Mikić*, 1995]. At this point, the system is still in equilibrium.

[13] In our idealized system the asymptotic wind speed is the same at all heliographic latitudes. In reality even the "steady" solar wind is more complex than this. At solar minimum, large polar coronal holes produce uniform high-speed wind at higher latitudes, whereas interaction regions (formed from the interaction of slow and fast streams) at low and middle latitudes are the site of slower and more variable wind. At solar maximum, on the other hand, smaller, middle or equatorial coronal holes produce intermediate, more variable speeds within relatively small volumes of the heliosphere, and slow and variable wind occupy the majority of space [e.g., *McComas et al.*, 2000]. The interaction of a flux rope with a more realistic ambient wind requires a three-dimensional treatment and will be the topic of a future study.

[14] In the bottom panel we show the simulated polarized brightness (pB). This was constructed by integrating the product of the number density with scattering function [*Billings*, 1966] along the line of sight. The resulting image bears a strong generic resemblance to SOHO/LASCO white-light images taken near solar minimum.

[15] Theories of flux rope CMEs generally start from the premise that CMEs are initiated by the release of energy stored in the coronal magnetic field [*Forbes*, 2000]. Previously, we have studied the possibility that eruptions could be initiated by photospheric motions that shear and twist the coronal magnetic field [*Mikić et al.*, 1988; *Linker and Mikić*, 1995, 1997; *Mikić and Linker*, 1994]. These results show that when the magnetic field is sheared beyond a critical value, helmet streamer configurations can erupt in a manner similar to "slow" CMEs, i.e., coronal mass ejections that are carried out of the corona by the solar wind. It has proven difficult to demonstrate that enough energy can be released rapidly enough by this mechanism to produce a "fast" CME that can drive an interplanetary shock. A more promising mechanism for producing fast CMEs is magnetic flux cancellation. We have found that a reduction in the magnetic flux (i.e., flux cancellation) near the neutral line of a sheared or twisted arcade configuration can lead to the formation of magnetic flux ropes [*Amari et al.*, 1999, 2000; *Linker et al.*, 2001a, 2001b]. When the flux cancellation reaches a critical threshold, the entire configuration erupts with the release of a considerable amount of magnetic energy.

[16] In the remaining two panels of Figure 1 we summarize the launch of just such a flux rope at 10 hours and 20 hours following the cancellation of flux. As can be seen, the origins of the the flux rope lie in the closed magnetic field lines embedded within the streamer belt. As the flux rope erupts into the solar corona, overlying field lines, which are still connected back to the Sun at both ends, are brought together under the flux rope. As they reconnect with each other, they contribute both to the flux of the evolving flux rope to the right of the reconnection site and to the regrowth of the streamer belt to the left. Note that the flux rope has developed an elliptical shape, with its major axis approximately horizontal. Note also that the reconnection site underneath the erupting flux rope is visible in the simulated pB image at $t = 20$ hours. This density enhancement was produced by the vertical (i.e., approximately parallel to the solar surface) flow of plasma into the reconnection region and has been observed in white light images [*Webb et al.*, 2002].

[17] With regard to the simulated polarized brightness images, we also remark that they bear a strong resemblance to the classic three-part structure of CMEs observed in white light. Specifically, the bright front, dark cavity, and dense core. Since this simulation was based on a polytropic approximation to the energy equation, associating the bright core with prominence material is, strictly speaking, not applicable. Nevertheless, when similar similar simulations, incorporating more realistic thermodynamics are run, the formation of a prominence is clearly seen [*Linker et al.*, 2001a, 2001b].

2.2. Evolution of the CME in the Solar Wind

[18] The plasma and magnetic field parameters from the outer boundary of the coronal model are used to drive the inner boundary of the heliospheric solution at 20 R_S. In Figure 2 we summarize the evolution of the flux rope and its associated distubances at 3 distances between the Sun and 1 AU ($\sim 215 R_S$). The snapshots were taken at times: 292, 304, and 320 hours following the start of the simulation. In this display we have combined results from both models. Number density contours are drawn in black and the colored contours refer to radial velocity. Magnetic field lines are shown in dark blue. The boundary between the two models is indicated by the thick white line at $20 R_S$. As can be seen, no obvious discontinuities are apparent. *Odstrcil et al.*

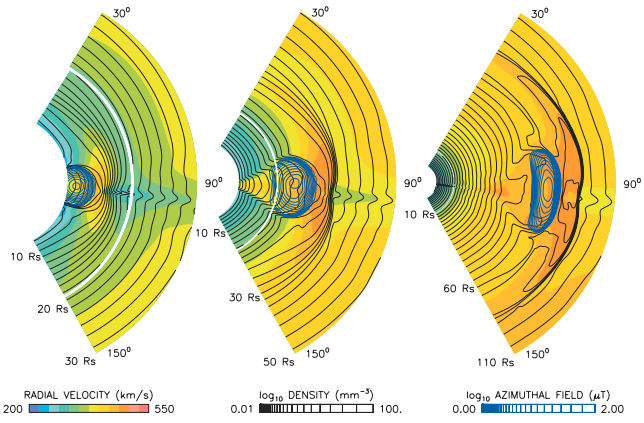

Figure 2. Evolution of the flux rope through the solar corona to ~0.5 AU. The panels extend ±60° in latitude and from left to right, extend in heliocentric distance from 10 R_S to 30 R_S, 50 R_S, and 110 R_S. The contours denote radial velocity (color); density (black lines); and magnetic field (blue lines). The interface between the coronal and heliospheric model is marked by the white line.

[2002] have analyzed the continuity of the solution at this interface in detail, concluding that no significant artifacts are introduced because of it. We note the following features in Figure 2. First, the initially elliptical flux rope becomes circular and then develops into a "pancake" structure. This is a combination of (1) kinematic expansion, as the ejecta moves into an ever larger spherical volume, and (2) dynamic evolution as the ejecta plows into slower ambient solar wind ahead. Second, a fast forward shock, driven by the ejecta, propagates poleward (as a wave) to the boundary of the calculation (±60° heliographic latitude). Third, both the shock and flux rope are beginning to develop concave-outward deformations in the vicinity of the plasma sheet, as they propagate through the denser medium [*Odstrcil et al.*, 1996].

[19] In Figure 3 we track the evolution of the ejecta and its associated disturbance between 1 AU and 5 AU. The snapshots were taken at times: 312, 360, and 696 hours following the start of the simulation. We have restricted the range in displayed speeds to 390–490 km s^{-1} to emphasize flows associated with the disturbance. Note how the ejecta becomes progressively more distorted with increasing helio-

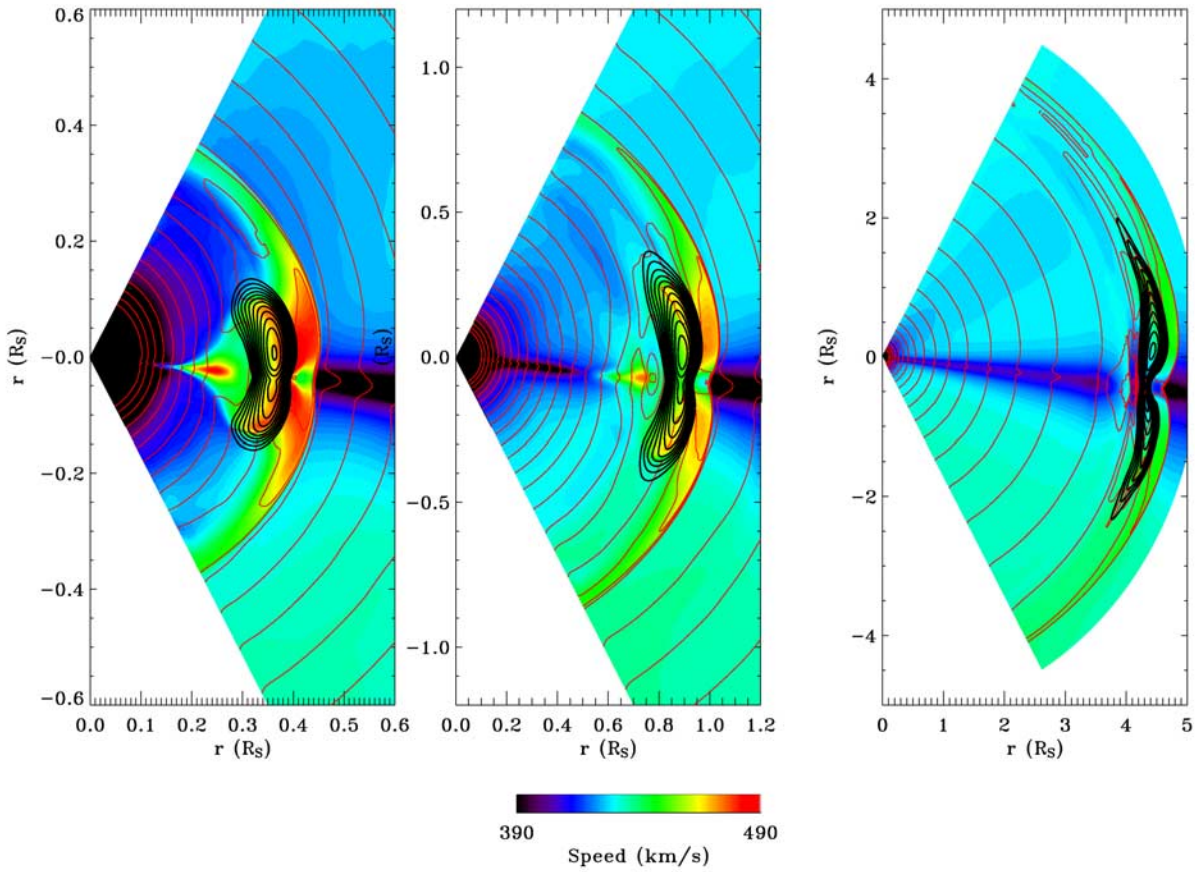

Figure 3. Evolution of the flux rope in the inner heliosphere. The panels extend ±60° in latitude and from left to right, extend in heliocentric distance from the Sun to 0.6 AU, 1.2 AU, and 5 AU. The contours denote radial velocity (color); density (red lines); and magnetic field (black lines).

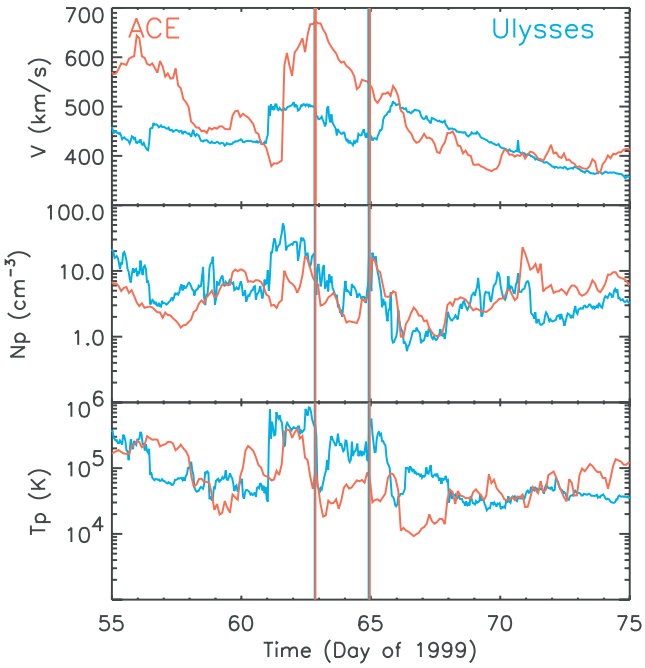

Figure 4. Comparison of speed, number density, and proton temperature at ACE (red) and Ulysses (blue). ACE data have been time-shifted and stretched such that the boundaries of the flux rope coincide with the boundaries determined at Ulysses. Vertical lines mark the boundaries of the ejecta as inferred from variations in the magnetic field vectors.

centric distance. By ~5 AU it has been squeezed so much at low latitudes that it has evolved into two lobes, connected by a thin band of compressed field. A detailed study of this aspect will be presented elsewhere. We can also identify outflow associated with posteruption reconnection underneath the flux rope, which has remained intact within the expansion wave (rarefaction region) behind the flux rope; it has a limited latitudinal extent (±15° and trails the ejecta by ~35R_S at 1 AU (middle panel). This aspect of the simulation is discussed in more detail by *Riley et al.* [2002].

3. Analysis of the In Situ Observations

[20] In late February 1999 the ACE spacecraft observed a flux-rope CME lasting for 21 hours. Thirteen days later Ulysses observed a flux-rope CME that lasted for 50 hours [*Lario et al.*, 2001]. At this time ACE was located at a heliocentric distance of 1 AU, very close to the ecliptic plane, while Ulysses was located at 22°*S*, 5 AU from the Sun, and at approximately the same heliolongitude as ACE. Although the plasma and magnetic profiles of these events were quite dissimilar, *Lario et al.* [2001] have argued that (1) the lack of multiple solar sources, (2) the longitudinal alignment, (3) the rotational orientations of the magnetic field, and (4) the average transit speed to both spacecraft support the conclusion that these were the same event. They suggested that Ulysses intercepted the cloud near its axis, while ACE crossed the cloud near its edge.

[21] In Figure 4 we summarize the main plasma observations at Ulysses and ACE. These were obtained from the SWOOPS [*Bame et al.*, 1992] and SWEPAM [*McComas et al.*, 1998] instruments, respectively. We have combined the observations at the two spacecraft by shifting the ACE data by 13.65 days and stretching it in time by a factor of 2.4, centered at 63.5 days. These values were derived from estimates of the boundaries of the ejecta observed at the two spacecraft. In addition, Ulysses measurements of density have been scaled by R^2 to account for the near adiabatic expansion of the solar wind. Note, however, that temperature has not been scaled.

[22] The boundaries of the ejecta at the two spacecraft were chosen principally by analyzing the magnetic field components (see below). Considering the ACE observations first, we note that the CME was traveling away from the Sun with an average speed of ~590 km s^{-1}. Based on its declining speed profile, it was clearly expanding. Because of its significantly faster speed than the ambient solar wind ahead, the ejecta can be seen to be driving a strong shock 1.25 (scaled) days ahead, consisting of a velocity jump of >200 km s^{-1}. The density and, to a lesser extent, temperature show a relative decrease within the ejecta, presumably the result of expansion. The profiles at Ulysses are qualitatively similar, although taken alone the comparison is not sufficiently close to infer that these are the same event. By the time the CME reached Ulysses, the average speed of the CME was ~460 km s^{-1}, and it was driving a wave ~2 days ahead, with a jump in speed of only ~70 km s^{-1}.

[23] Next we consider the magnetic field measurements in Figure 5 in the usual spacecraft-centered rtn coordinate system, where **r** points radially away from the Sun, **t** lies

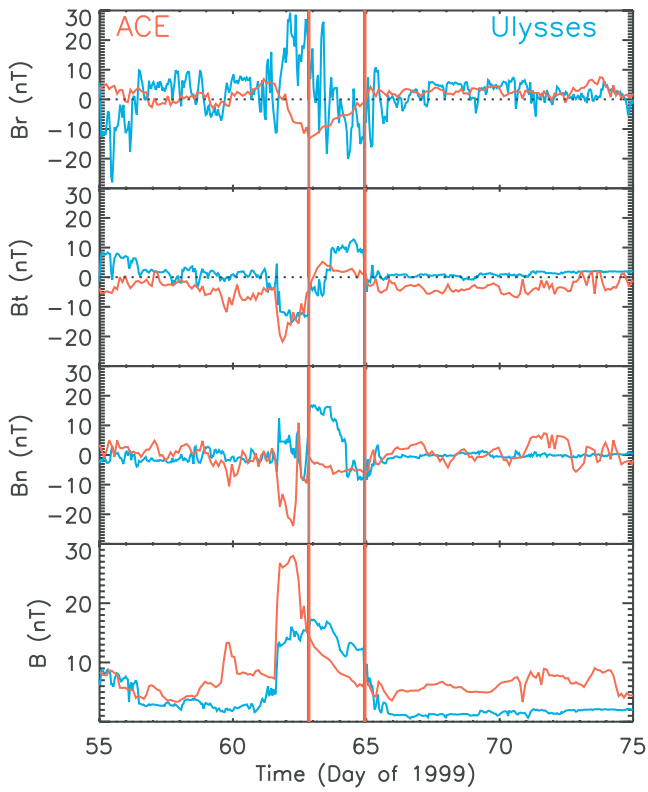

Figure 5. Same format as Figure 4, showing magnetic field components (r, t, and n) and magnitude.

Table 1. Force-Free Fitting Parameters for Flux Ropes Observed at ACE and Ulysses[a]

Parameter	ACE	Ulysses
Start, day hr:min	49 14:00	62 20:00
Stop, day hr:min	50 11:00	64 22:00
Φ, deg	282.1	271.1
Θ, deg	−1.3	53.0
y/*R*	0.738	0.0064
Helicity	−1	−1
R, AU	0.28	0.34

[a]See text for details.

in the equatorial plane and points into the direction of planetary motion (i.e., the azimuthal coordinate), and **n** completes the right-handed system. Again, we have time shifted and stretched the ACE observations [*Smith et al.*, 1998] so that they lie over the Ulysses measurements [*Balogh et al.*, 1992]. At Ulysses, B_r has been scaled by R^2, while B_t and B_n have been scaled by R. The boundaries of the flux ropes (summarized in Table 1) were deduced by considering each event individually and looking at the variations in the magnetic field, as described by *Lepping et al.* [1990] for example. We note the coincidental lineup of discontinuities in the magnetic field magnitude at the location of the forward shock preceding the event at ACE (day 61.7). Based on analysis of the plasma data, it is likely that the real shock jump is a much more modest event ~3/4 day earlier, and that this coincidental jump is only a discontinuity. Comparison of the magnetic field rotations within the CMEs reveal notable differences. At ACE, B_r shows a coherent rotation from a negative value to zero, whereas the same component at Ulysses remains essentially zero (the random fluctuations are amplified because of the R^2 scaling). The component B_t at ACE begins slightly negative and transitions through zero, peaking before the temporal midpoint of the event, and falling to zero by the end. At Ulysses, B_t also rotates from a negative value to a maximum positive number, which it maintains during the second half of the cloud before dropping sharply to zero. Finally, B_n remains essentially zero at ACE, whereas at Ulysses it displays a rise from zero to a maximum, followed by a fall back to zero. The magnitude of the field both at ACE and Ulysses shows a relatively monotonic decrease from the leading edge to the trailing edge.

[24] In Figure 6 we compare ACE [*Gloecler et al.*, 1998] and Ulysses [*Gloeckler et al.*, 1992] composition measurements from the two spacecraft using the same shift and stretch as for Figure 4. The top panel compares the ratio of helium to protons (He++/H+), as measured by the SWOOPS (Ulysses) and SWEPAM (ACE) plasma instruments. The middle panel shows the ratio of O^{7+} to O^{6+}) and the bottom panel shows the average charge state of iron (⟨QFe⟩) as measured by the SWICS instruments. The O7/O6 ratios are a good measure of the oxygen freeze-in temperature in the lower corona. Average Fe charge states, on the other hand provide a proxy measure of the coronal source temperature: Values of 10–11 suggest a temperature of 1 MK, whereas values of 16 suggests a much hotter ~5 MK environment. The He++/H+ ratios at the two spacecraft show similar increases from about 4% to 8 or 9% above the ambient values. The average Fe charge states also track reasonably well both inside the event and in the surrounding ambient wind. Most interesting, however, are the O7/O6 ratios, which differ substantially at the two spacecraft, both during the ejecta interval and for a period of 1.5–2 days preceding it. In the case that both ejecta are the same event (see discussion below), the fact that the Oxygen freeze-in temperature within the CME was substantially higher at ACE than at Ulysses, implies a clear spatial (latitudinal) inhomogeneity.

[25] We can estimate the time taken for the disturbance observed at ACE to travel to the location of Ulysses, assuming radial propagation and constant deceleration. The average speed of the CME at ACE was ~590 km s^{-1}, while the CME at Ulysses was traveling at ~460 km s^{-1}. Thus assuming a constant deceleration of the ejecta between 1 and 5 AU suggests a transit time between the two spacecraft of 13.6 days. This corresponds well with the measured transit time of 13.9 days, reinforcing the idea that these events were one and the same. Moreover, with the assumption of approximately radial propagation, this suggests that the ejecta was moving at approximately the same radial speed at different latitudes.

3.1. Force-Free Fitting of the In Situ Observations

[26] We have computed the basic flux rope parameters for the events at ACE and Ulysses assuming the the flux ropes were force free and thus describable by a cylindrically symmetric magnetic field solution [*Lepping et al.*, 1990]. Table 1 summarizes these parameters. Considering the events individually first, we surmise that ACE intercepted a flux rope with a negative helicity, 74% away from its magnetic axis. This axis lies essentially in the equatorial plane and points approximately perpendicular to

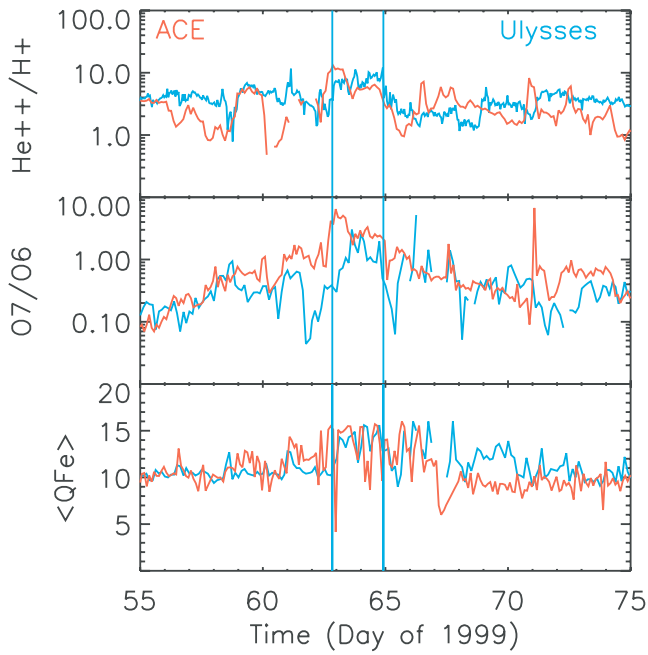

Figure 6. Same format as Figure 4, showing the ratio of He++/H+, O7/O6, and the average charge state of Iron (⟨QFe⟩).

the radial direction. The event at Ulysses also had a negative helicity, but the spacecraft traveled to within 1% of its magnetic axis. Again the magnetic axis lay approximately perpendicular to the radial direction but in this case was tilted significantly in the meridional direction. By including velocity measurements, the inferred radial size of the flux rope at ACE was 0.28 AU, while at Ulysses it was 0.34 AU (a ~20% difference).

3.2. Comparison of MHD Results With In Situ Observations

[27] By flying the ACE and Ulysses trajectories through the simulation results we can make direct comparisons with the in situ observations. We reiterate that this is a generic simulation and not constructed to quantitatively mimic any specific event. We believe, however, that it contains the basic qualitative features of many CMEs in the solar wind. In Figure 7 we compare speed, density, temperature, magnetic field strength and directions from ACE (top left) and Ulysses (bottom left) with simulation results (top right and bottom right, respectively). Based on the force-free fittings at the two spacecraft discussed earlier, we infer that ACE intercepted the CME near its flank, whereas Ulysses intercepted it closer to the axis, suggesting that the centroid of the CME was displaced significantly southward of the equator. In our simulation, however, the axis of the CME was displaced southward by a modest ~10°. Thus to make more meaningful comparisons with the observations, we extracted ACE profiles at 18°N and Ulysses profiles at 2°N. In essence, then, we have reversed the relative latitudinal positions of the spacecraft in the simulation.

[28] Comparison of the simulation results with the in situ observations reveal a number of similarities, yet the generic nature of the model also necessarily leads to a number of discrepancies. We focus first on the observed variables at ACE. As we have noted earlier, the ejecta was traveling significantly faster than the ambient solar wind (~590 kms^{-1} at 1 AU) and drove a relatively strong shock. The density and temperature profiles did not show large dips within the ejecta, typically indicative of expansion. The magnetic field within the ejecta showed little systematic variation. Of some note, however, is the small rotation in the radial component of the field. The magnetic field strength decreased from the leading edge to the trailing edge and was maximum in the sheath region preceding the ejecta, both aspects resulting from the fast speed of the ejecta relative to the ambient solar wind. The simulation results mimic the speed profile fairly well. This would be expected, since any expanding ejecta traveling faster than the ambient solar wind will drive a wave/shock ahead and present a decreasing speed profile within the ejecta. The temperature, density, and field component profiles, while not inconsistent, do not have any definitive features that we can associate with the observations. Variations in the simulated magnetic field components are also low, with the largest changes occurring in the sheath region. Finally, the magnetic field magnitude, while enhanced within the ejecta, does not have the characteristic peak in the sheath region, which, as we have noted, is due to the more modest velocity difference between the simulated ejecta and the ambient wind ahead.

[29] At Ulysses the ejecta is inferred to be expanding and presumably driving the shock at the beginning of day 61. This basic profile is mimicked in the simulation results. Note that the observed shock boundary is distinct from the magnetic discontinuity (marked "d") later on day 61 and suggests that the interaction between the ejecta and the ambient solar wind was more complex than the simpler picture suggested by the simulation. Turning to a comparison of the magnetic field vectors, we note that the large-scale rotations in all components are mimicked well by the simulations, in particular (1) the flat B_r profile, (2) the rise and fall in B_t, and (3) the rotation from positive to negative values in B_n. Finally, the magnetic field strength compares quite favorably, with a relatively flat (or slightly falling) profile within the ejecta and more rapid fall off behind. Comparison of either the observed or simulated magnetic field strength profiles at the two spacecraft suggests that this was a strongly magnetic structure at Ulysses but less so at ACE.

4. Summary and Discussion

[30] In this study we have analyzed ACE and Ulysses observations of a CME within the context of a global MHD model. Based on the analysis of possible solar sources and the magnetic field rotations, together with timing arguments, *Lario et al.* [2001] suggested that the same CME was observed by both spacecraft. The results of the global MHD simulation presented here support this scenario. We have computed the force-free parameters for the event at each spacecraft. Detailed comparisons of plasma, magnetic field, and composition measurements are, for the most part, qualitatively similar. The ratio O7/O6, however, shows significant differences, suggesting that if they are the same CME, strong spatial inhomogeneities existed within the flux rope back at the Sun.

[31] If we are to believe the force-free results, then given the inferred size of the flux rope at the two spacecraft and their latitudinal separation, it is unlikely that the two spacecraft could have intercepted the same event and we are led to a picture of two distinct events, as summarized in Figure 8a. Yet whether or not the events observed at ACE and Ulysses were the same, the mere fact that the ejecta were faster than the surrounding medium suggests that they must have been significantly more compressed in the radial direction than the circular cross sections that are intrinsic to the force-free method. This is an important point that is often overlooked when analyzing such events: if the flux rope is propagating faster than the ambient solar wind ahead, it will develop a pancake-like shape. In addition, since the scale size of the event is determined by a radial slice (i.e., the spacecraft's trajectory through the ejecta), the fitting procedure necessarily underestimates the true size of the event. For the simulation presented here the extent of the ejecta in the radial direction is only 20% of its latitudinal extent.

[32] On the other hand, using the MHD results to interpret the ACE and Ulysses observations suggests a fundamentally different picture of the flux rope and its associated disturbance. When we add the additional evidence that the transit time from one spacecraft to the

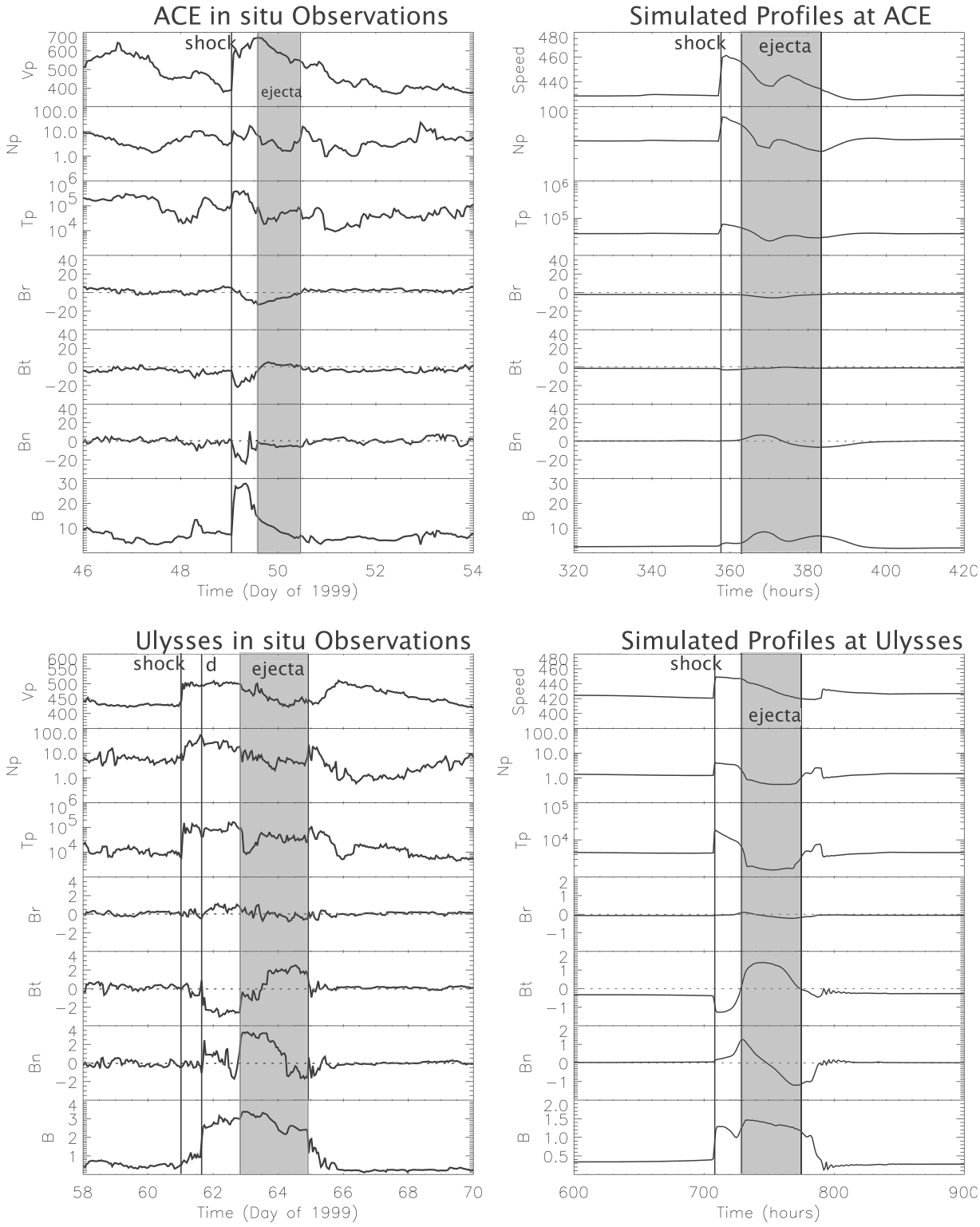

Figure 7. Comparison of observed plasma and magnetic field parameters (left) with simulated parameters (right).

other agrees remarkably well with a simple calculation of the transit time based on constant deceleration and further that there was only one obvious disturbance back at the Sun that could be associated with both events [*Lario et al.*, 2001], we are led to the conclusion that the same CME was observed by the two spacecraft. Thus the picture we propose to account for event is shown in Figure 8b.

[33] Two aspects of our analysis, however, do not immediately fit with the "single event" hypothesis. First, the Θ

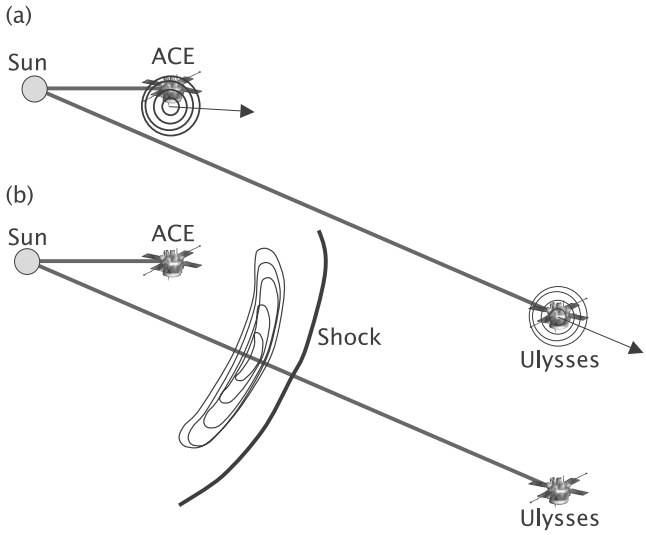

Figure 8. Schematic showing the picture of the ACE/Ulysses event(s) as inferred from (a) force-free modeling and (b) MHD modeling.

force-free parameter at Ulysses was calcuated to be 53° (Table 1), suggesting that the axis of the flux rope was rotated significantly away from the ecliptic plane. In contrast, at ACE this angle was close to zero. Second, measurements of O7/O6 showed significant differences at the two spacecraft. Taken in isolation, these differences might lend support for the "multiple event" scenario. However, given the larger body of evidence discussed above, we propose alternative explanations for these apparent discrepancies.

[34] To account for the nonalignment of the flux rope axes at ACE and Ulysses, we believe three-dimensional geometric or dynamical effects were present that cannot be accounted for in our two-dimensional model. It is possible, for example, that the limited longitudinal extent of a real CME combined with intrinsic spatial variations in azimuth could lead to such differences. It is also possible that ambient solar wind structure preceeding the ejecta could deform it in such a way to account for this.

[35] With regard to the differences in O7/O6 at the two spacecraft, we first note that our single-fluid MHD model does not address these measurements in any meaningful way. Although we are clearly far from understanding the solar processes responsible for the relative abundances of these heavier ions, we can nevertheless appreciate their importance as tracers of solar wind source regions. The interpretation of the composition measurements observed at ACE and Ulysses has significant implications. If we believe that the same event was observed at both spacecraft, then the observed differences suggest significant spatial inhomogenieties within an individual CME. This may provide an alternative interpretation for the results by *Neukomm* [1998], who found that statistically, CMEs observed at high heliographic latitudes (the so-called "over-expanding" CMEs [*Gosling et al.*, 1994] had O7/O6 ratios that tended to be lower than CMEs observed near the ecliptic plane. An obvious interpretation of Neukomm's result is that "over-expanding" CMEs are a distinct class of CME (essentially, the view that the events seen at ACE and Ulysses are unrelated). An alternative interpretation based on the present study is that CMEs are spatially inhomogenious in latitude and that the over-expanding events were merely the higher-latitude flanks of larger structures. While we could only speculate on possible mechanisms on coronal loops that would give such a spatial variability, clearly the implications are important.

[36] Although the current two-dimensional model has been relatively successful in reproducing the essential features of the in situ observations at ACE and Ulysses and providing a global context for them, three-dimensional effects are undoubtedly important and should be considered in the future. Perhaps surprisingly, the fact that this event was observed near solar maximum added to the successfulness of the comparison. Since the large-scale ambient solar wind was dominated by slow and intermediate-speed flow, interaction regions were not as pronounced as they would have been during the declining phase and surrounding solar minimum. Our neglect of the third dimension, however, seriously limits our abilities to probe the connectivity of the magnetic field lines making up the flux rope with the Sun. In two dimensions, all flux rope field lines are completely disconnected from the Sun. In contrast, observations of counterstreaming suprathermal electrons within CMEs [e.g., *Gosling et al.*, 1987] indicate that a significant fraction of these field lines are still connected back to the Sun at both ends. In fact, field lines totally disconnected from the Sun, although sometimes present, are a relatively rare occurrence [e.g., *Gosling et al.*, 1995].

[37] Although the simulation has provided an important global context for interpreting these observations, it has failed to reproduce several components of the observations. The causes of these errors can be traced to a combination of approximations in the model. Perhaps most fundamentally, we do not know the underlying mechanism for the eruption of CMEs at the Sun. We believe that the "flux cancellation" model described and implemented here is a promising candidate: it is broadly consistent with a range of remote solar observations prior to and during the eruption of a CME and produces flux ropes that have properties matching both solar and in situ observations of CMEs, at least in a generic sense. Thus far, however, it has proven difficult to generate ejecta with sufficiently large speeds to match the fast CMEs observed in the solar wind. Indeed, the comparison at ACE in Figure 7 (top panels) would have been greatly enhanced if the eruption mechanism had generated a CME traveling at say 700 kms^{-1} near the Sun. We are currently investigating ways of producing faster CMEs. A second approximation is the neglect of variations in the azimuthal direction. By doing so, the axis of the flux rope was and remained in the azimuthal direction. Our force-free analysis (Table 1), however, clearly showed that at Ulysses the axis was tilted substantially away from this direction. Whether this was an initial condition of the flux rope or the result of interacting with a structured ambient solar wind is unclear. We have begun to simulate the eruption of CMEs in three dimensions and we will explore this added complexity in the near future.

[38] While our analysis has highlighted some of the dangers in over-interpreting force-free fittings, we emphasize that this approach retains many useful features. In particular, the orientation of the flux rope axis and the sense of the helicity retain their meaning. On the other hand, for fast CMEs and particularly those driving a shock, the inferred size, impact parameter, and integrated helicity must be interpreted with some care. Recently, these kinematic models have been extended to include expansion effects [*Marubashi*, 1997], the relaxation of the force-free assumption [*Farrugia et al.*, 1995], and two-spacecraft fittings [*Mulligan et al.*, 2001]. However, it remains to be seen how the types of dynamic deformations described here impact these approaches.

[39] In closing, we remark that given the idealized nature of the simulation, it is quite remarkable that so much complexity is generated. Moreover, since only a single simulation was performed (with no optimization of boundary or initial conditions) we are encouraged that such simulations will be a useful aid for interpreting observations of magnetic clouds. Future studies that extend the simulation to three dimensions will allow us to explore the connectivity and topology of magnetic field lines within and surrounding the ejecta and may eventually provide constraints on CME eruption mechanisms. Composition and charge state measurements provide a powerful and largely underutilized diagnostic tool to probe the birth sites of CMEs and their role as tracers should also be incorporated into future modeling efforts.

[40] **Acknowledgments.** The authors gratefully acknowledge the support of the National Aeronautics and Space Administration (Living with a Star Program, Sun-Earth Connections Theory Program, and Supporting Research and Technology Programs) and the National Science Foundation (SHINE Program and the Center for Integrated Space Weather Modeling) in undertaking this study. We also thank National Science Foundation at the San Diego Supercomputer Center and the National Energy Research Supercomputer Center for providing computational support.

[41] Shadia Rifai Habbal thanks Joan Feynman and James A. Klimchuk for their assistance in evaluating this paper.

References

Amari, T., T. Boulmezaoud, and Z. Mikić, An interactive method for the reconstruction of the solar coronal magnetic field. 1. method for regular solutions, *Astron. Astrophys.*, *350*, 1051, 1999.

Amari, T., J. F. Lucini, Z. Mikić, and J. A. Linker, A twisted flux rope model for coronal mass ejections and two-ribbon flares, *Astrophys. J.*, *529*, L49, 2000.

Balogh, A., T. J. Beek, R. J. Forsyth, P. C. Hedgecock, R. J. Marquedant, E. J. Smith, D. J. Southward, and B. T. Tsurutani, The magnetic field investigation on the Ulysses mission: Instrumentation and preliminary scientific results, *Astron. Astrophys*, *92*, 221, 1992.

Bame, S. J., D. J. McComas, B. L. Barraclough, J. L. Phillips, K. J. Sofaly, J. C. Chavez, B. E. Goldstein, and R. K. Sakurai, The Ulysses solar wind plasma experiment, *Astron. Astrophys., Suppl. Ser.*, *92*, 237, 1992.

Cargill, P. J. J. Schmidt, D. S. Spicer, and S. T. Zalesak, Magnetic structure of over expanding coronal mass ejections: Numerical models, *J. Geophys. Res.*, *105*, 7509, 2000.

Farrugia, C. J., V. A. Osherovich, and L. F. Burlaga, Magnetic flux rope versus the spheromak as models for interplanetary magnetic clouds, *J. Geophys. Res.*, *100*, 12,293, 1995.

Forbes, T., A review on the genesis of coronal mass ejections, *J. Geophys. Res.*, *105*, 23,153, 2000.

Gloeckler, G., et al., The solar wind ion composition spectrometer, *Astron. Astrophys., Suppl. Ser.*, *92*, 267, 1992.

Gloekler, G., et al., Investigation of the composition of solar and interstellar matter using solar wind and pickup ion measurements with SWICS and SWIMS on the ACE spacecraft, *Space Sci. Rev.*, *86*, 495, 1998.

Gosling, J. T., D. N. Baker, S. J. Bame, W. C. Feldman, and R. D. Zwickl, Bidirectional solar wind electron heat flux events, *J. Geophys. Res.*, *92*, 8519, 1987.

Gosling, J. T., D. J. McComas, J. L. Phillips, L. A. Weiss, V. J. Pizzo, B. E. Goldstein, and R. J. Forsyth, A new class of forward-reverse shock pairs in the solar wind, *Geophys. Res. Lett.*, *21*, 2271, 1994.

Gosling, J. T., J. Birn, and M. Hesse, Three-dimensional magnetic reconnection and the magnetic topology of coronal mass ejection events, *Geophys. Res. Lett.*, *22*, 869, 1995.

Hundhausen, A. J., The origin and propagation of coronal mass ejections, in *Solar Wind 6*, edited by V. J. Pizzo, T. E. Holzer, and D. G. Sime, *Tech. Note NCAR-TN-306+Proc*, p. 306, Natl. Cent. for Atmos. Res., Boulder, Colo., 1988.

Klimchuk, J. A., Theory of coronal mass ejections, in *Space Weather*, *Geophys. Monogr. Ser.*, vol. 125, edited by P. Song, H. Singer, and G. Siscoe, pp. 143, AGU, Washington, D. C., 2001.

Lario, D., D. K. Haggerty, E. C. Roelof, S. J. Tappin, R. J. Forsyth, and J. T. Gosling, Joint Ulysses and ACE observations of a magnetic cloud and the associated solar energetic particle event, *Adv. Space Sci.*, *97*, 277, 2001.

Lepping, R. P., J. A. Jones, and L. F. Burlaga, Magnetic field structure of interplanetary magnetic clouds at 1 AU, *J. Geophys. Res.*, *95*, 11,957, 1990.

Linker, J. A., and Z. Mikić, Disruption of a helmet streamer by photospheric shear, *Astrophys. J.*, *438*, L45, 1995.

Linker, J. A., and Z. Mikić, Extending coronal models to Earth orbit, in *Coronal Mass Ejections*, *Geophys. Monogr. Ser.*, vol. 99, edited by N. Crooker, J. A. Joselyn, and J. Feynman, pp. 269, AGU, Washington, D. C., 1997.

Linker, J. A., et al., Magnetohydrodynamic modeling of the solar corona during Whole Sun Month, *J. Geophys. Res.*, *104*(A5), 9809, 1999.

Linker, J. A., et al., Magnetohydrodynamic modeling of the solar corona during Whole Sun Month, *J. Geophys. Res.*, *104*, 9809, 2001a.

Linker, J. A., R. Lionello, Z. Mikić, and T. Amari, Magnetohydrodynamic modeling of prominence formation within a helmet streamer, *J. Geophys. Res.*, *106*, 25,165, 2001b.

Lionello, R., Z. Mikić, and D. D. Schnack, Magnetohydrodynamics of solar coronal plasmas in cylindrical geometry, *J. Comput. Phys.*, *140*, 172, 1998.

Lionello, R., Z. Mikić, and J. A. Linker, Stability of Algorithms for Waves with Large Flows, *J. Comp. Phys.*, *152*, 346, 1999.

Marubashi, K., Interplanetary magnetic flux ropes and solar filaments, in *Coronal Mass Ejections*, *Geophys. Monogr. Ser.*, vol. 99, edited by N. Crooker, J. A. Joselyn, and J. Feynman, pp. 147, AGU, Washington, D. C., 1997.

McComas, D. J., S. J. Bame, P. Barker, W. C. Feldman, J. L. Phillips, P. Riley, and J. W. Griffee, Solar wind electron proton alpha monitor (SWEPAM) for the Advanced Composition Explorer, *Space Sci. Rev.*, *86*, 563, 1998.

McComas, D. J., J. T. Gosling, and R. M. Skoug, Ulysses observations of the irregularly structured mid-latitude solar wind during the approach to solar maximum, *Geophys. Res. Lett.*, *27*, 2437, 2000.

Mikić, Z., and J. A. Linker, Disruption of coronal magnetic field arcades, *Astrophys. J.*, *430*, 898, 1994.

Mikić, Z., J. A. Linker, D. D. Schnack, R. Lionello, and A. Tarditi, Magnetohydrodynamic modeling of the global solar corona, *Phys. Plasmas*, *6*, 2217, 1999.

Mulligan, T., C. T. Russell, B. J. Anderson, and M. H. Acuna, Multiple spacecraft flux rope modeling of the Bastille Day magnetic cloud, *Geophys. Res. Lett.*, *28*, 4417, 2001.

Odstrcil, D., Interactions of solar wind streams and related small structures, *J. Geophys. Res.*, *99*, 17,653, 1994.

Odstrcil, D., and M. Karlicky, Triggering of magnetic reconnection in the current sheet by shock waves, *Astron. Astrophys.*, *326*, 1252, 1997.

Odstrcil, D., and M. Karlicky, Interaction of shocks with a current sheet and reconnection in the solar corona, *Advances Space Res.*, *19*, 1895, 2000.

Odstrcil, D., and V. J. Pizzo, Three-dimensional propagation of CMEs in a structured solar wind flow: 1. CME launched within the streamer belt, *J. Geophys. Res.*, *104*, 483, 1999a.

Odstrcil, D., and V. J. Pizzo, Three-dimensional propagation of CMEs in a structured solar wind flow: 2. CME launched adjacent to the streamer belt, *J. Geophys. Res.*, *104*, 493, 1999b.

Odstrcil, D., and V. J. Pizzo, Distortion of the interplanetary magnetic field by three-dimensional propagation of coronal mass ejections in a structured solar wind, *J. Geophys. Res.*, *104*, 28,225, 1999c.

Odstrcil, D., M. Dryer, and Z. Smith, Propagation of an interplanetary shock along the heliospheric plasma sheet, *J. Geophys. Res.*, *101*, 19,973, 1996.

Odstrcil, D., J. A. Linker, R. Lionello, Z. Mikić, P. Riley, V. J. Pizzo, and J. Luhmann, Merging of coronal and heliospheric numerical 2-D MHD models, *J. Geophys. Res.*, *107*(A12), 1493, doi:10.1029/2002JA009334, 2002.

Riley, P., and J. T. Gosling, Do coronal mass ejections implode in the solar wind?, *Geophys. Res. Lett.*, *25*, 1529, 1998.

Riley, P., J. T. Gosling, and V. J. Pizzo, A two-dimensional simulation of the radial and latitudinal evolution of a solar wind disturbance driven by a fast, high-pressure coronal mass ejection, *J. Geophys. Res.*, *102*, 14,677, 1997.

Riley, P., J. A. Linker, Z. Mikić, D. Odstrcil, V. J. Pizzo, and D. F. Webb, Evidence of post-eruption reconnection associated with coronal mass ejections in the solar wind, *Astrophys. J.*, *578*, 972, 2002.

Smith, C. W., J. L'Heureux, N. F. Ness, M. H. Acuna, L. F. burlaga, and J. Scheifele, The ACE magnetic field experiment, *Space Sci. Rev.*, *86*, 613, 1998.

Vandas, M., and D. Odstrcil, Magnetic cloud evolution: A comparison of analytical and numerical solutions, *J. Geophys. Res.*, *105*, 12,605, 2000.

Vandas, M., D. Odstrcil, and S. Watari, Three-dimensional MHD simulation of a loop-like magnetic cloud in the solar wind, *J. Geophys. Res.*, *107*(A9), 1236, doi:10.1029/2001JA005068, 2002.

D. Lario, Applied Physics Laboratory, Johns Hopkins University, Laurel, MD 20723, USA. (david.lario@jhuapl.edu)

R. P. Lepping, Laboratory for Extraterrestrial Physics, NASA Goddard Space Flight Center, Greenbelt, MD 20771, USA. (Ron.Lepping@gsfc.nasa.gov)

J. A. Linker, Z. Mikić, and P. Riley, Science Applications International Corporation, San Diego, CA 92121, USA. (linker@iris023.saic.com; mikic@iris023.saic.com; pete.riley@saic.com)

D. Odstrcil, NOAA/Space Environment Center, Boulder, CO 80305, USA. (Dusan.Odstrcil@noaa.gov)

T. H. Zurbuchen, Department of Atmospheric, Oceanic and Space Sciences, University of Michigan, Ann Arbor, MI 48109, USA. (thomasz@umich.edu)